Recurrent slope failure enhancing source rock burial depth and seal unit competence in the Pearl River Mouth Basin, offshore South China Sea

Fang Zhao[1,4], Tiago M. Alves[2], Wei Li[3 *], Shiguo Wu[1*]

[1] Key Laboratory of Marine Geology and Environment, Institute of Oceanology, Chinese Academy of Sciences, Qingdao, China

[2] 3D Seismic Lab. School of Earth and Ocean Sciences, Cardiff University, Main Building, Park Place, Cardiff, CF10 3AT, United Kingdom

[3] MARUM, Center for Marine Environmental Sciences, University of Bremen, Bremen, Germany

[4] University of Chinese Academy of Sciences, Beijing 100049, China. E-mail address: wli@marum.de (Wei Li), swu@qdio.ac.cn (Shiguo Wu)

Abstract

High quality 3D seismic data are used to assess the significance of mass-transport deposits (MTDs) to the evolution of the Pearl River Mouth Basin (South China Sea). Basal shear surfaces and lateral margins of seven recurrent MTDs are mapped to reveal a general NE-SW transport direction throughout the Late Miocene-Quaternary. A key result of our analysis is the perceived relationship between the recurrence of slope instability in the study area and the Dongsha Tectonic Event. Using borehole data to constrain the ages of interpreted MTDs, we show that tectonic uplift in the northern South China Sea led to the oversteepening of the slope in the Late Miocene (between 10.5 Ma and 5.5 Ma), preconditioning the continental slope to fail recurrently for a period >10 Ma. Interpreted MTDs are shown to enhance burial depths of source and reservoir units, and improve seal competence in lower slope areas. Conversely, upper slope regions record important erosion and reduced sealing capacity in Late Cenozoic strata. As a result, we postulate that the thickness variations imposed by MTDs on Late Miocene-Quaternary strata have important implications to petroleum plays in the South China Sea.

Keywords: Continental margins; South China Sea; Mass-transport deposits; Faults; Burial depth; Petroleum plays

1. Introduction

Mass-transport deposits (MTDs) are ubiquitous on continental margins and play a vital role in redistributing vast amounts of sediment into deep-water areas (Masson et al., 2006, Bull et al., 2009). Recent data have also demonstrated that MTDs provide an important contribution to slope architecture and infill on both passive and tectonically active continental margins (Bache et al., 2011; Strasser et al., 2011). In these settings, MTDs can comprise reliable stratigraphic markers of tectonic activity. For instance, MTDs appear to be reliable markers of breakup events on continental margins (Soares et al., 2014). They are also reliable markers of seafloor uplift and deformation on any tectonic setting (Alves et al., 2014). Significantly, MTDs comprising mud prone successions or homogeneous debris flows can act as seal units for underlying petroleum reservoirs (Moscardelli et al., 2006).

The northern South China Sea is a key area in SE Asia where MTDs are known to accumulate on the outer shelf and continental slope areas (Li et al., 2014). Possible triggers of mass-wasting include high sedimentation rates, abrupt sea level variations and, as argued in this paper, slope oversteepening and enhanced seismic activity during the Dongsha Tectonic Event. As one of the most effective methods to recognise both buried and modern MTDs (e.g. Gong et al., 2014), 3D seismic data is used in this paper to investigate a series of MTDs located in the southwest part of the Dongsha Uplift (Fig. 1b). We use a high-quality 3D seismic data, tied to borehole stratigraphic information, to demonstrate that the Pearl River Mouth Basin experienced three main episodes of tectonic uplift during the Cenozoic; the Nanhai, the Baiyun and the Dongsha Events (Dong et al., 2009). While the Nanhai and Baiyun tectonic events are well documented in the literature, little is known about the

Dongsha Event and its impact on offshore basins of South China Sea. The aims of this study are thus: 1) to briefly describe the recurrent MTDs observed in the Pearl River Mouth Basin; 2) to estimate the age of these recurrent MTDs; 3) to tentatively correlate these MTDs with a major tectonic event in the South China Sea, i.e. the Dongsha Event; and 4) to discuss the influence of these MTDs (and associated tectonic event) on petroleum systems of the Pearl River Mouth Basin.

2. Data and methods

The interpreted 3D seismic volume was acquired and processed by China National Offshore Oil Corporation. The volume is located southwest of the Dongsha Islands (Fig. 1a), in water depths between 1400 m and 1800 m (Fig. 1b). It covers an area of approximately 600 km^2 with a bin size of 12.5 m×12.5 m. Its frequency bandwidth ranges from 45 to 100 Hz with a dominant frequency of 75 Hz. Average vertical resolution for the studied interval is 8-10 m.

Borehole LW 6-1-1 and data from four other industry wells were used to tie nine stratigraphic unconformities to the seismic data (Figs. 1c and d; Sun et al., 2013; Wu et al., 2014). In parallel, three key horizons (Horizon 1 to 3) were mapped in detail. Time structure maps of basal shear surfaces were extracted from the 3D seismic dataset to characterize the source areas and geometries of MTDs.

Different fault families were identified on coherence data and manually mapped. In parallel, throw-depth (t-z) techniques were used to analyze the propagation histories of Late Cenozoic faults in the study area (e.g. Baudon and Cartwright, 2008).

3. Geological setting

As one of the largest and deepest marginal seas in the SE Asia, the South China Sea records complex tectonic events that reflect its location between the Eurasian, Pacific and Australia-India plates (Briais et al., 1993). The Pearl River Mouth Basin lies on the northeastern continental margin of the South China Sea, and spans an area larger than 40,000 km^2 (Fig. 1a). The Pearl River Mouth Basin is one of the most prolific hydrocarbon-rich basins of the South China Sea (Dong et al. 2009; Zhu et al. 2009). Its geological evolution can be divided into three main phases (Gong et al. 1989): (1) early continental rifting and onset of subsidence (Late Cretaceous-Early Oligocene); (2) syn-rift faulting, subsidence and deposition within distinct sub-basins (Late Oligocene-Early Miocene); and (3) post-rift subsidence and infill of the entire basin, occurring from the Mid Miocene onwards. Rifting in the South China Sea began during the Nanhai Event, which occurred ~32 Ma ago (Dong et al., 2009). The Baiyun episode took place at ~23 Ma, and separates syn-rift from post-rift sequences (Dong et al., 2009). After seafloor spreading ceased at ~16.5 Ma, shallow marine deposits dominated the subsequent deposition of the Hanjiang Formation. In such a setting, the Dongsha Event occurred in the Late Miocene (10.5-5.5 Ma) and ceased around the Miocene/Pliocene boundary (5.5 Ma) (Wu et al., 2014; Zhao et al., 2012). The Dongsha Event resulted in generalised uplift of the northern slopes of the South China Sea, upper crust faulting, erosion and in widespread magmatism. These phenomena are thought to have played an important role in the evolution of petroleum systems throughout the northern continental slope of the South China Sea (Lüdmann et al., 2001). After the Dongsha Event, the Yuehai and Wanshan Formations deposited open shelf and deltaic deposits (Fig. 1c).

4. Internal character, geometry and estimated age of recurrent MTDs

Interpreted MTDs comprise highly discontinuous to chaotic strata overlying laterally continuous reflections (e.g. Bull et al., 2009). A total of seven MTDs, occurring at different depths, are observed within Late Miocene to Quaternary sedimentary units (Fig. 2a). The vast majority of the mapped MTDs occur within Unit 2 (Late Miocene) (Fig. 2a).

The 3D seismic data were used to characterize the internal structure and kinematic indicators of three major MTDs in Unit 2, MTD 1, MTD 2 and MTD 3, and four stacked MTDs below. The headwall scarps of these MTDs are not imaged due to the limited coverage of the 3D seismic volume, but they were likely generated in upper slope regions of the Dongsha Uplift. MTD 1 extends almost continuously along the continental slope (Fig. 2a). MTD 1 is the youngest mass-transport deposit interpreted and occurs ~45 m below the modern seafloor. In contrast, MTD 2 is observed within uppermost Miocene strata (Fig. 2a). It shows an average thickness of 50 m and disappears

gradually downslope. MTD 3 is located below MTD 2 and its thickness shows striking spatial variations (Figs. 2a). It thickens towards the centre of the study area and, conversely, thins progressively downslope (Fig. 2a).

In addition to MTDs 1 to 3, at least four stacked MTDs are observed within the base of Late Miocene strata (Fig. 2a). They appear to be separated by thin, but well-stratified, intervals (Figs. 1d and 2a). These stacked MTDs are cut by numerous faults and named in this paper as Mass-Wasting Complex A (Fig. 2a). Most of these faults have lower tips terminating below the base of MTD 3 (Figs. 2a and b).

Recurrent MTDs are chiefly sourced from Late Miocene strata as indicated by seismic-well ties their age are constrained and estimated from the seismic-stratigraphy (Fig. 2a). Mass-Wasting Complex A began to develop at around 10.5 Ma (T2). MTD 3 accumulated later around the same location, denoting the stacking of more than 160 m of sediment in a short space of time. At the end of the Miocene, MTD 2 was deposited above MTD 3, whilst MTD 1 is likely younger than 5.5 Ma (T1).

5. Origin of recurrent MTDs and their potential impact on petroleum systems

The basal shear surfaces of MTD 1 to 3 are coincident with Horizons 1 to 3, respectively (Fig. 2a). Horizons 1 to 3 comprise continuous seismic reflections separating highly deformed sediments (MTDs) from undeformed strata below (Fig. 2a). Time structure maps from Horizon 1 to 3 show that they are deeper in the northeast compared to the southwestern part of the study area (Figs. 3a, b and c). The lateral margins of MTDs 1 to 3 are shown on time structure maps and on key seismic profile (Fig. 4a). The geomorphology of Horizon 1 to 3 and directions of the lateral margins reveal a NE to SW transport direction for MTDs 1 to 3. We therefore estimate that the interpreted MTDs were derived from the upper slope area to the northeast of the study area.

Gas fields, including the Panyu Uplift gas field, the Wenchang gas field and the LW3-1 gas field, have been discovered in the Pearl River Mouth Basin in the past two decades (Pang et al., 2006; Zhu et al., 2009). The likely source intervals for these gas fields occur in the Enping (Eocene) and Wenchang Formations (early Oligocene) (Fig. 1c; Huang et al., 2003; Zhu et al., 2009). The principal Eocene source rock is a coal-bearing sequence accumulated under fluvial, swamp and shallow lacustrine environments (Huang et al., 2003). Early Oligocene source rock comprises marine black shales with a total thickness of several hundred meters (Huang et al., 2003). During the Oligocene and Miocene, massive sandstone reservoirs developed in the Oligocene Zhuhai Formation and in the Miocene Zhujiang Formation. Older reservoir intervals are also known in the Oligocene Enping Formation and in the upper Miocene Yuehai Formation (Zhu et al., 2009).

The study area is located southwest of the region affected by the Dongsha Event within a continental slope depocentre dominated by recurrent mass-wasting (Figs. 1a and c). As MTDs have been considered as reliable proxies for tectonic activity on several continental margins (Alves et al., 2014; Ruano et al., 2014), we focus this discussion on four stacked MTDs that began to develop at around 10.5 Ma. The well-constrained dates for these stacked MTDs, between 8 Ma and 10.5 Ma based on borehole data (Figs. 1d and 2a) are consistent with the onset of the Dongsha Event (Pin et al., 2001; Wu et al., 2014). This event has been interpreted to be associated with subduction of the South China Sea slab beneath the Philippine Sea Plate at the Manila trench. After subduction of lower density crust within the continental-ocean transition zone was initiated, large resistance stresses may have led to lithosphere bending and crustal uplift in the Dongsha area (Wu et al., 2014). In addition, active faults related to Dongsha Event are widely observed in the study area. Most faults propagate vertically from the crest of uplifted horst, and their upper tips terminate below the base of MTD 3 - except for one single fault cutting through MTD 3 in Fig. 4b. Some fault scarps were also reactivated as compressional structures ('pop-up structures'), forming small scale folds at the base of MTD 3 (Fig. 4c). These structures provide strong evidence that faulting in the study area was still active after the formation of MTD 3.

An important observation on seismic data is the significant thickness of MTDs interpreted in the study area, between 310 m and 640 m, whereas erosional areas on the upper slope are expected to have thinner Late Miocene-Quaternary strata in response to the uplift of the Dongsha High (Fig. 6a). We interpret this setting to have important implications to petroleum systems in the Pearl

River Mouth Basin, as shown in Figure 6. Tectonic tilting of the margin, and associated faulting, was likely responsible for enhanced fluid migration throughout the South China Sea. At the same time oversteepening and erosion of the upper slope region occurred, a significant thickness of MTDs was accumulated in mid- to lower-slope regions, leading to an increase in burial depth in Cenozoic strata capping hydrocarbon-rich intervals (Fig. 1d). This interpretation is corroborated by the 1D models in Fig. 6, which demonstrate higher degrees of maturity for strata below stacked MTDs in Site B. We therefore favour a setting in which the fast, and widespread accumulation of MTDs in the Late Miocene increased the potential for maturation (and trapping) of hydrocarbons in perched slope depocentres, whereas regions uplifted by local tectonics saw their seal (and burial) potential reduced. A corollary of this interpretation is that similar regions to the Pearl River Mouth Basin, recording local uplift events, may also record enhanced petroleum potential in mid- to lower slope areas where recurrent MTDs have accumulated. In contrast, source areas of MTDs coincide with regions of marked tectonic uplift, reflecting diachronous tectonic events along the full extent of the South China Sea from South Vietnam to Northern Taiwan.

Acknowledgements

We are grateful to China National Offshore Oil Corporation for their permission to release the seismic data. This research was financially supported by National Basic Research Program of China (No. 2015CB251201) and Key Project of Natural Science Foundation of China Foundation (No. 91228208). Laurent Jolivet and an anonymous reviewer are thanked for their thorough reviews and constructive comments which greatly improved this manuscript.

References

Alves, T.M., Strasser, M., Moore, G.F., 2014. Erosional features as indicators of thrust fault activity (Nankai Trough, Japan). Marine Geology.

Bache, F., Leroy, S., Baurion, C., Robinet, J., Gorini, C., Lucazeau, F., Razin, P., d'Acremont, E., Al-Toubi, K., 2011. Post-rift uplift of the Dhofar margin (Gulf of Aden). Terra Nova 23, 11-18.

Baudon, C., Cartwright, J., 2008. The kinematics of reactivation of normal faults using high resolution throw mapping. Journal of Structural Geology 30, 1072-1084.

Briais, A., Patriat, P., Tapponnier, P., 1993. Updated interpretation of magnetic anomalies and seafloor spreading stages in the south China Sea: Implications for the Tertiary tectonics of Southeast Asia. Journal of Geophysical Research: Solid Earth 98, 6299-6328.

Bull, S., Cartwright, J., Huuse, M., 2009. A review of kinematic indicators from mass-transport complexes using 3D seismic data. Marine and Petroleum Geology 26, 1132-1151.

Dong, D., Zhang, G., Zhong, K., Yuan, S., Wu, S., 2009. Tectonic evolution and dynamics of deepwater area of Pearl River Mouth basin, northern South China Sea. Journal of Earth Science 20, 147-159.

Gong, C., Wang, Y., Hodgson, D.M., Zhu, W., Li, W., Xu, Q., Li, D., 2014. Origin and anatomy of two different types of mass-transport complexes: A 3D seismic case study from the northern South China Sea margin. Marine and Petroleum Geology.

Gong, Z.S., Jin, Q., Qiu, Z., Wang, S., Meng, J., 1989. Geology tectonics and evolution of the Pearl River Mouth Basin, in X. Zhu, ed., Chinese sedimentary basins: Amsterdam, Netherlands, Elsevier, p. 181-196.

Hu, D., Zhou, D., Wu, X., He, M., Pang, X., Wang, Y., 2009. Crustal structure and extension from slope to deepsea basin in the northern South China Sea. Journal of Earth Science 20, 27-37.

Huang, B., Xiao, X., Zhang, M., 2003. Geochemistry, grouping and origins of crude oils in the Western Pearl River Mouth Basin, offshore South China Sea. Organic Geochemistry 34, 993-1008.

Lüdmann, T., Kin Wong, H., Wang, P., 2001. Plio–Quaternary sedimentation processes and neotectonics of the northern continental margin of the South China Sea. Marine Geology 172, 331-358.

Li, P., 1993.Cenozoic tectonic movement in the Pearl River Mouth Basin. China Offshore Oil Gas (Geology) 7, 11–17 (In Chinese with English abstract).

Li, W., Wu, S., Wang, X., Zhao, F., Wang, D., Mi, L., Li, Q., 2014. Baiyun Slide and Its Relation to Fluid Migration in the Northern Slope of Southern China Sea, in: Krastel, S., Behrmann, J.-H., Völker, D., Stipp, M., Berndt, C., Urgeles, R., Chaytor, J., Huhn, K., Strasser, M., Harbitz, C.B. (Eds.), Submarine Mass Movements and Their Consequences. Springer International Publishing, pp. 105-115.

Masson, D.G., Harbitz, C.B., Wynn, R.B., Pedersen, G., Lovholt, F., 2006. Submarine landslides: processes, triggers and hazard prediction. Philos Trans A Math Phys Eng Sci 364, 2009-2039.

Moscardelli, L., Wood, L., Mann, P., 2006. Mass-transport complexes and associated processes in the offshore area of Trinidad and Venezuela. AAPG Bulletin 90, 1059-1088.

Pang, X., Chen, C.M., Zhu, M., 2006. A discussion about hydrocarbon accumulation conditions in the Baiyun deep-water area, northern

continental slope, South China Sea (in Chinese): China Offshore Oil & Gas 18, 145-149.

Pin, Y., Di. Z., Zhaoshu, L., 2001. A crustal structure profile across the northern continental margin of the South China Sea. Tectonophysics 338, 1-21.

Ruano, P., Bohoyo, F., Galindo-Zaldívar, J., Pérez, L.F., Hernández-Molina, F.J., Maldonado, A., García, M., Medialdea, T., 2014. Mass transport processes in the southern Scotia Sea: Evidence of paleoearthquakes. Global and Planetary Change, in press.

Soares, D.M., Alves, T.M., Terrinha, P., 2014. Contourite drifts on early passive margins as an indicator of established lithospheric breakup. Earth and Planetary Science Letters 401, 116-131.

Strasser, M., Moore, G.F., Kimura, G., Kopf, A.J., Underwood, M.B., Guo, J., Screaton, E.J., 2011. Slumping and mass transport deposition in the Nankai fore arc: Evidence from IODP drilling and 3-D reflection seismic data. Geochemistry, Geophysics, Geosystems 12, Q0AD13.

Sun, Q., Cartwright, J., Wu, S., Chen, D., 2013. 3D seismic interpretation of dissolution pipes in the South China Sea: Genesis by subsurface, fluid induced collapse. Marine Geology 337, 171-181.

Wu, S., Gao, J., Zhao, S., Lüdmann, T., Chen, D., Spence, G., 2014. Post-rift uplift and focused fluid flow in the passive margin of northern South China Sea. Tectonophysics 615-616, 27-39.

Zhao, S.J., Wu, S.G., Shi, H.S., Dong, D.D., Chen, D.X., Wang, Y., 2012. Structures and dynamic mechanism related to the Dongsha Event at the northern margin of the South China Sea. Prog. Geophys. 27, 1008e1019.

Zhu, W., Huang, B., Mi, L., Wilkins, R.W.T., Fu, N., Xiao, X., 2009. Geochemistry, origin, and deep-water exploration potential of natural gases in the Pearl River Mouth and Qiongdongnan basins, South China Sea. AAPG Bulletin 93, 741-761.

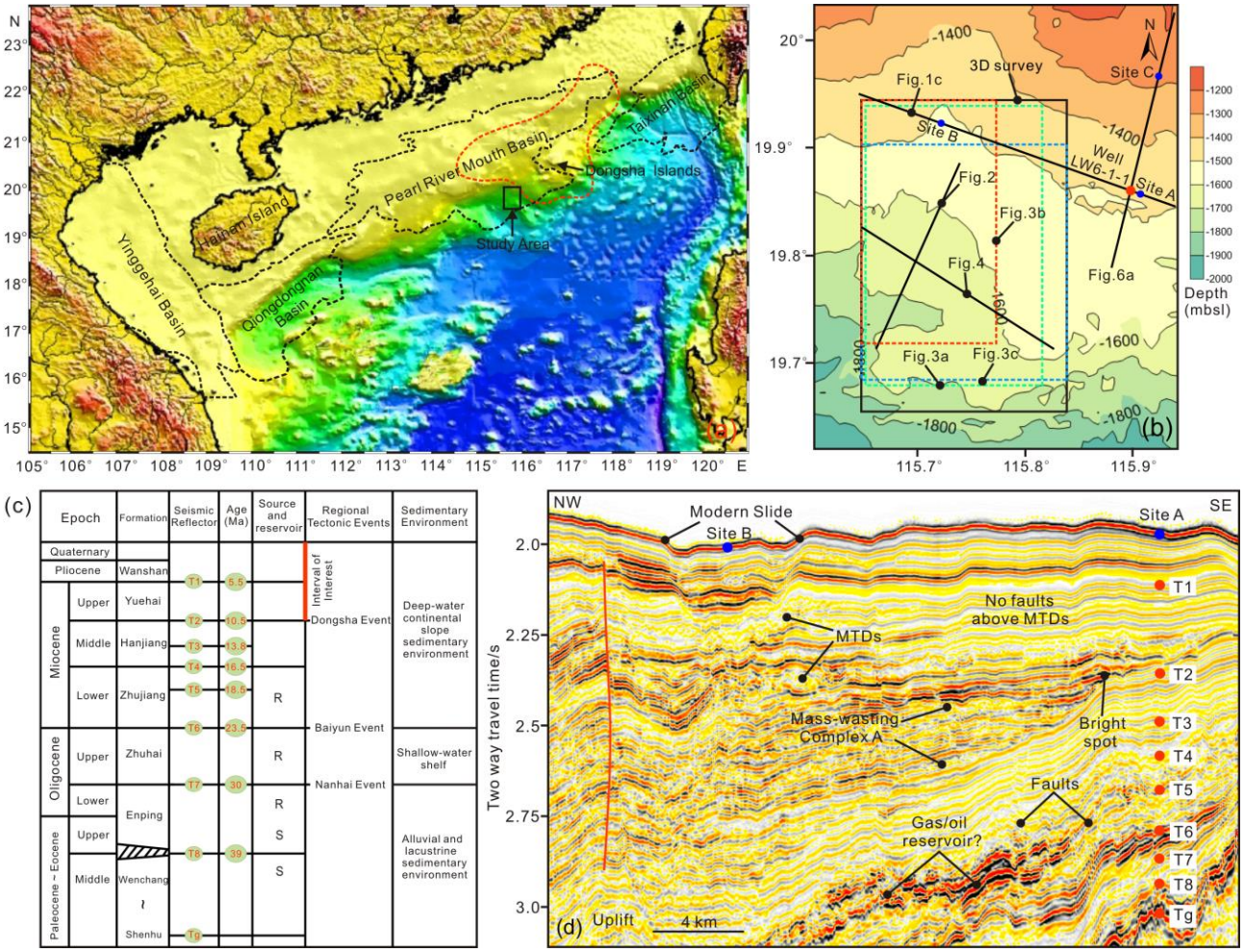

Figure 1 - (a) Combined bathymetric and topographic map showing the locations of major Cenozoic basins in the northern South China Sea. The black box indicates the study area. The red dotted line represents the region affected by Dongsha Event (modified after Sun et al., 2013; Wu et al., 2014; Zhao et al., 2012). (b) Depth contour map of the study area (See location in Fig.1a). The black box marks the location of 3D seismic volume. Black solid lines highlight the profiles interpreted in this paper. The location of well LW6-1-1 used to constrain the seismic stratigraphy in the study area is also shown. (c) Schematic stratigraphic columns of the Pearl River Mouth Basin showing source rock, reservoir, tectonic event and sedimentary environment (modified after Li, 1993).(d) 2D seismic profile across MTD-prone regions in the Pearl River Mouth Basin showing eight main seismic sequences. The ages of the seismic surfaces are determined from Well LW6-1-1 and data from Sun et al. (2013) and Wu et al. (2014). Note the presence of a Mass-Wasting Complex A within Late Miocene strata (between T1 and T2) deposited above a brightened interval, likely to comprising hydrocarbon accumulations.

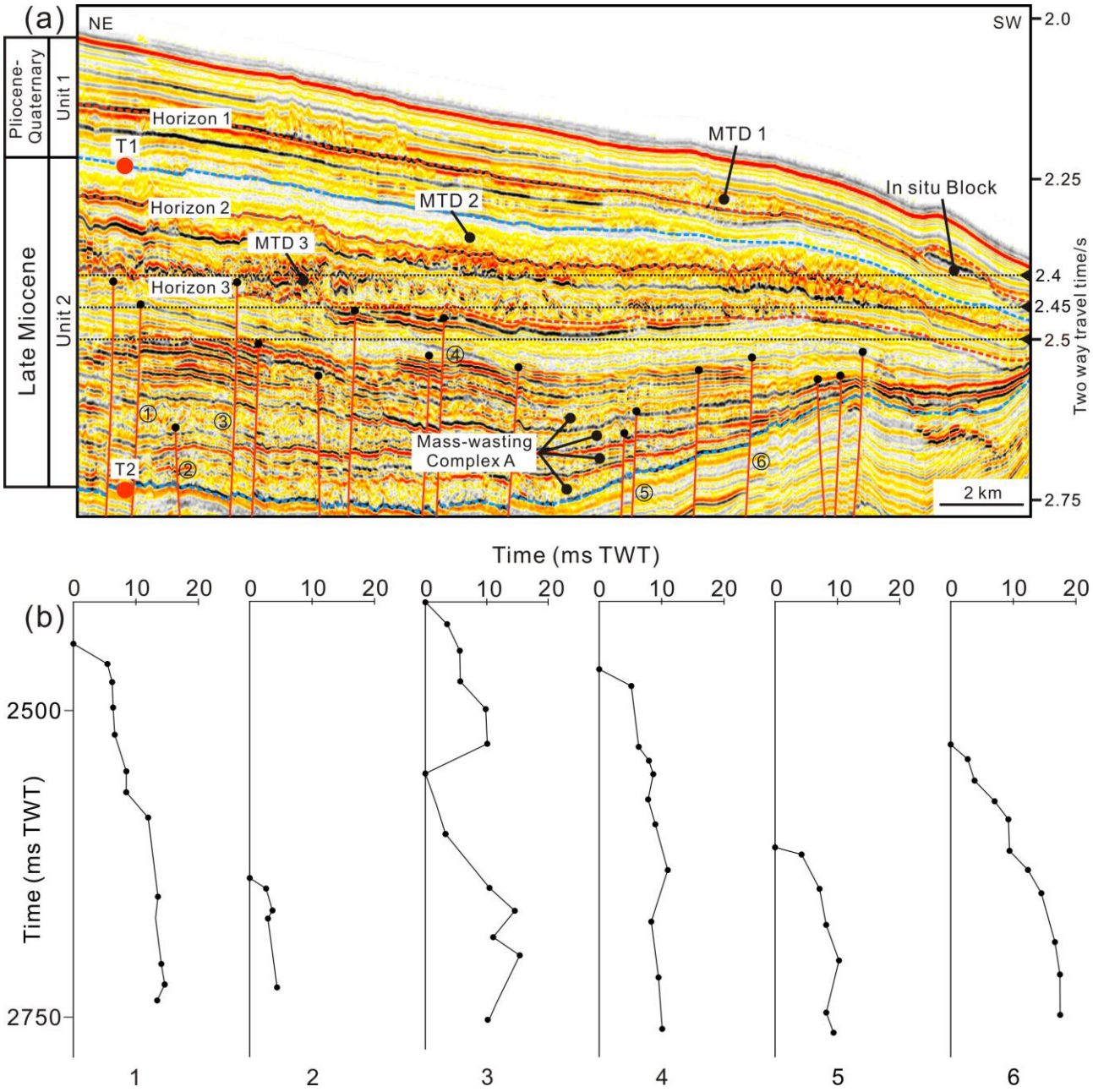

Figure 2 - (a) 3D seismic profile across the continental slope showing MTD 1 to 3 and Mass-Wasting Complex A. Horizon 1 to Horizon 3 represent the basal shear surfaces of MTD 1, MTD 2 and MTD 3, respectively. The three coherence slices Fig. 5 are shown as dashed lines at 2400 ms, 2450 ms and 2500 ms, respectively. Faults are label by red solid lines and their upper tip are marked by black dots. (b) Throw-Depth graphs for six representative faults in the study area. The positions of the faults are labeled in Fig.1b.

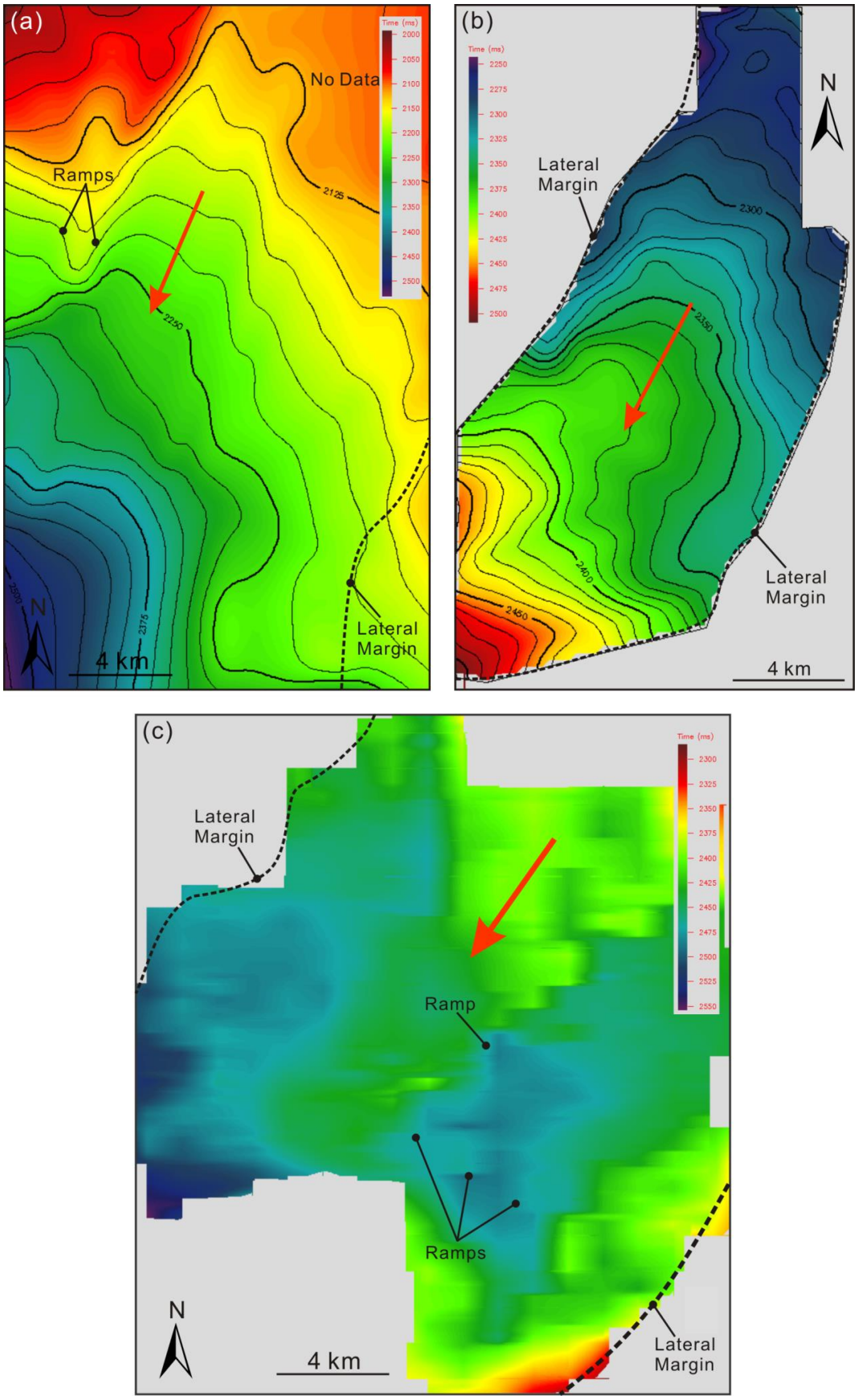

Figure 3 - Time structure map of the basal shear surface of a) MTD 1, b) MTD 2 and c) MTD 3 taken from the interpreted 3D seismic data (location shown in Fig.1b). Dashed lines represent the lateral margins of MTDs. Red arrows indicate mass transport direction. Steep basal ramps and lateral margins are also shown.

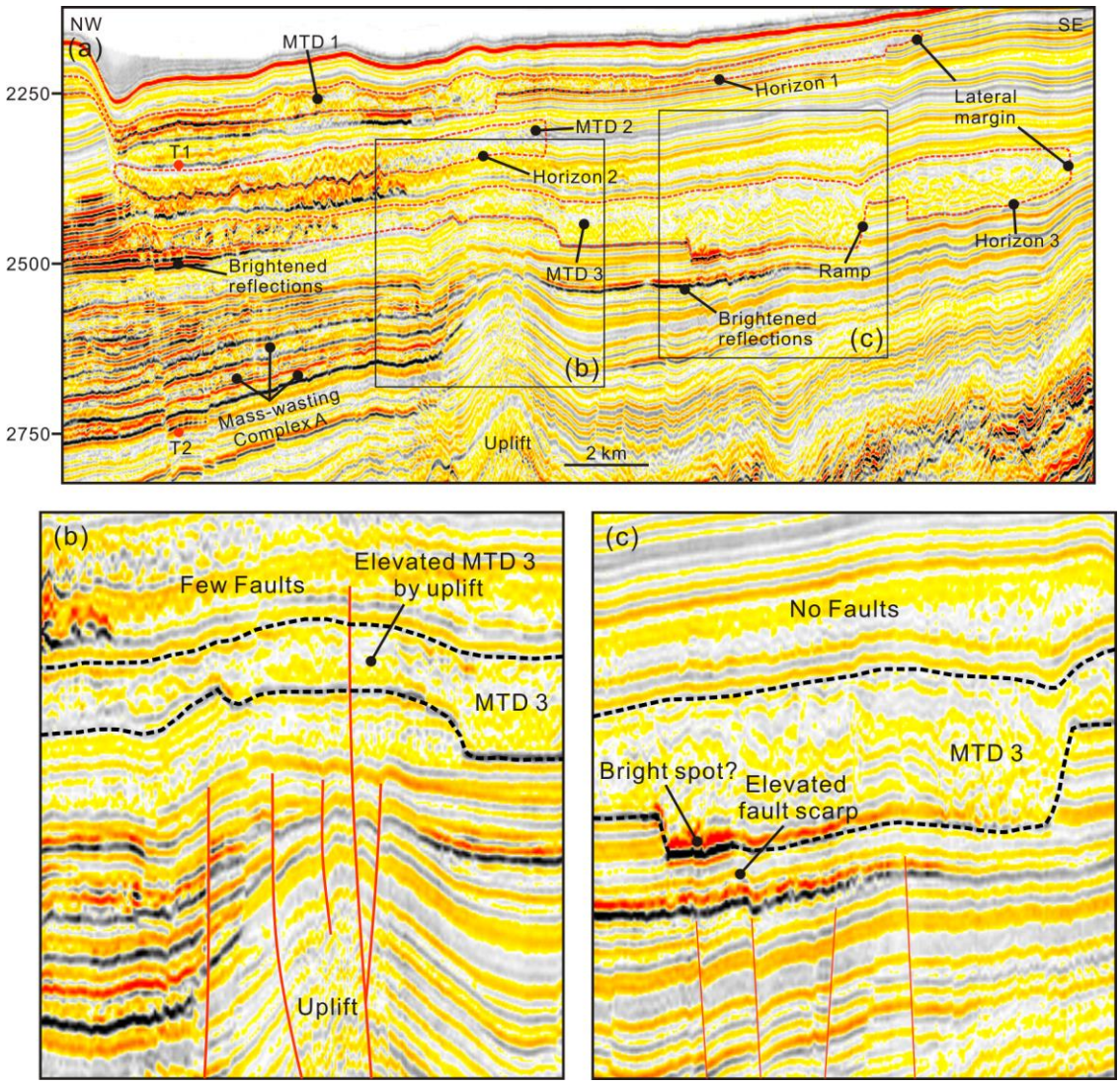

Figure 4 - (a) 3D seismic lines across the MTDs depicting basal ramps, lateral margins and basal shear surfaces in some of the interpreted MTDs. (b) Zoomed section showing MTD 3 uplifted and intersected by a single fault. (c) Zoomed seismic profile showing the basal shear surface of MTD 3 and strata above the upper tip of one fault reactivated to form a small-scale 'pop-up' structure. The strata below the base of MTD 3 were cut by several faults, while no faults were identified above its upper boundary.

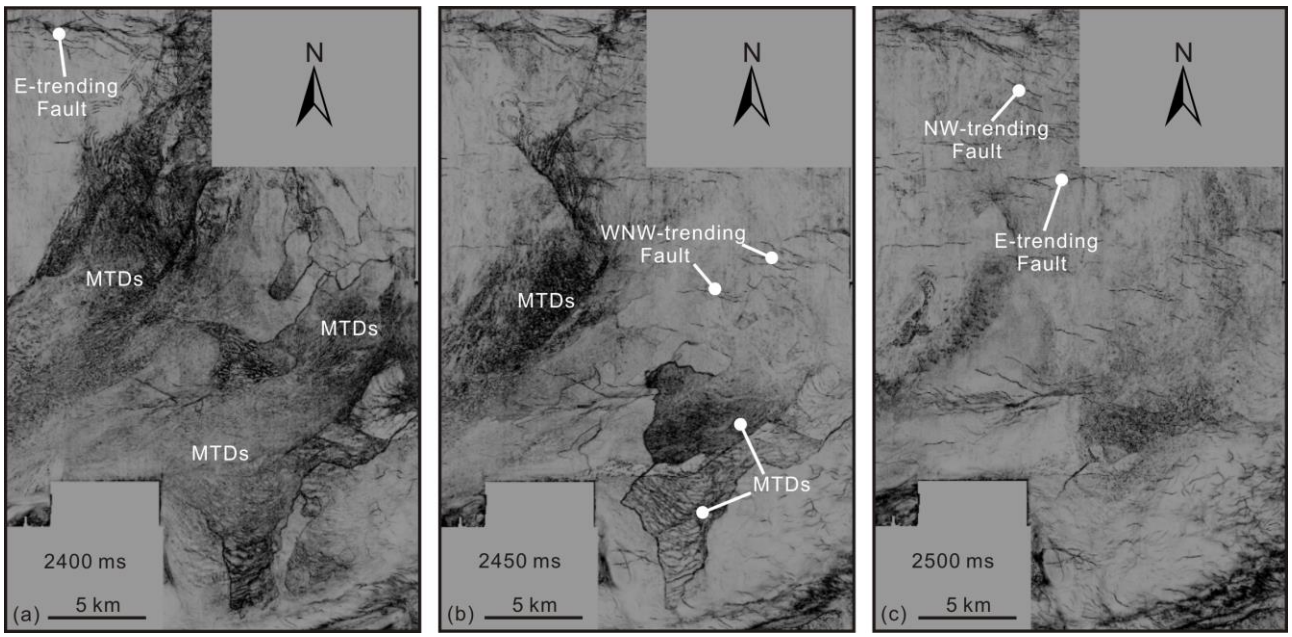

Figure 5 - (a) Coherence slice at 2400 ms (TWT, within the MTD 3 strata) showing widespread MTDs and E-trending faults in the northwest corner of the 3D seismic volume where no MTDs are observed.. (b) Coherence slice at 2450 ms (within the MTD 3 strata) shows small scale MTDs and WNW-trending faults. (c) coherence slice taken at 2500 ms (below the base of MTD 3) shows NW-trending and E-trending faults. The relative depths of Figs. 5a, b and c are shown in Fig. 2a.

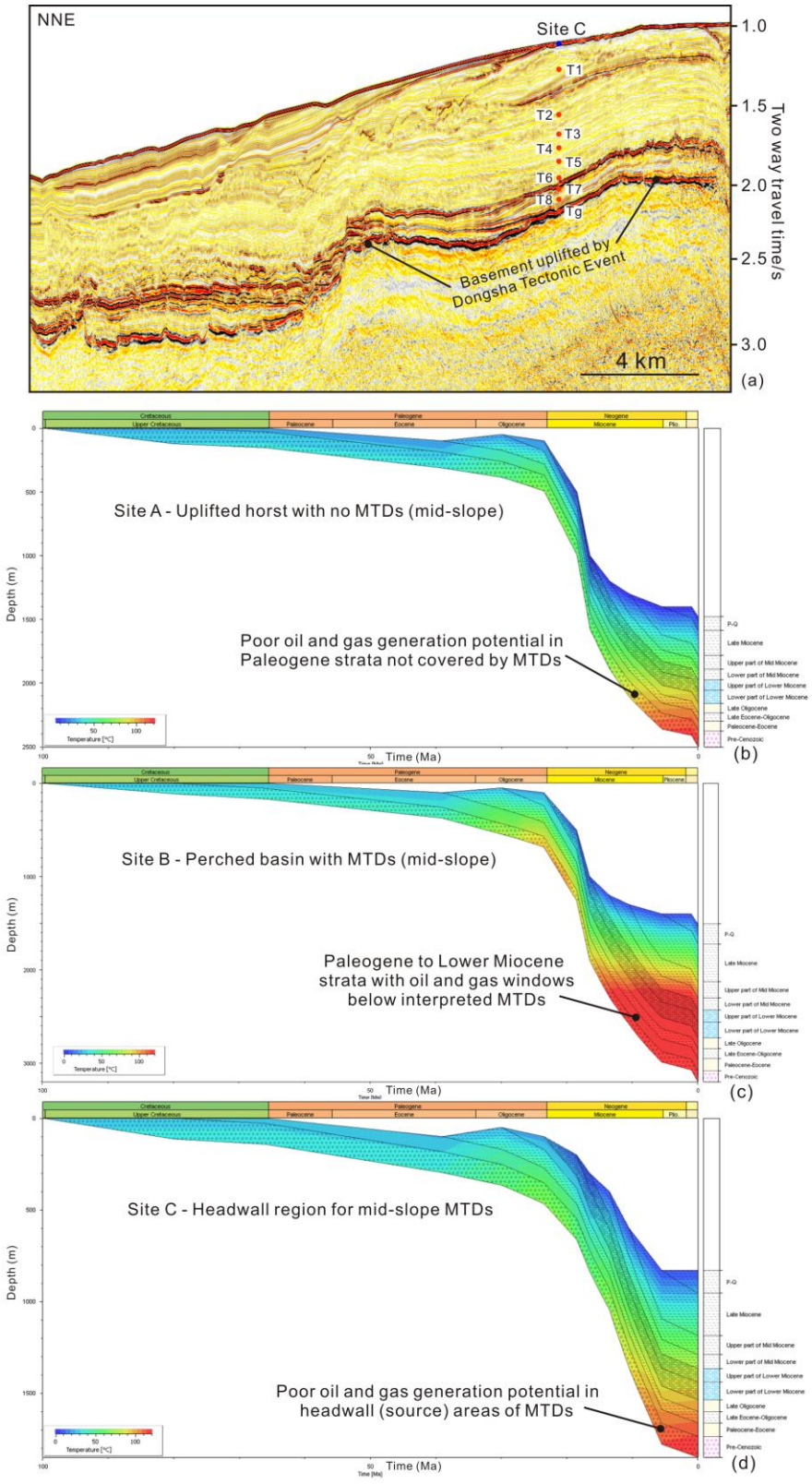

Figure 6 - PetroMod temperature models for Sites A, B and C, shown in Figure 1b. Horizons T1 to Tg were tied to borehole LW6-1-1 shown in the same figure. Heat flow values were based on a crustal thickness of 16 km and a mantle depth of 20 km, based on the published literature (Hu et al., 2009)**.** The syn-rift event was considered to happen from 28 Ma to 20 Ma before present, for beta values of 3.00 and 5.00 for crust and mantle units, respectively. (a) 2D seismic line across the source area of recurrent MTDs. Basement highs were uplifted by Dongsha Event. (b) 1-D temperature model for Site A. (c) 1-D temperature model for Site B. (d) 1-D temperature model for Site C. Temperature scale bars highlight in red the depths and timings in which the gas window was reached, i.e. T>90^{o}C.